Recent Advances in Hybrid Imaging for Radiation Therapy Planning: The Cutting Edge

Habib Zaidi, PhD, PD[a,b,*], Tinsu Pan, PhD[c]

KEYWORDS

• PET/CT • Radiation therapy • Treatment planning
• Respiratory motion • Image segmentation

PET/CT for radiation therapy planning (RTP) has been reported,[1–5] and it is expected that PET/CT will play an important role in the future of RTP or biologically guided radiation therapy (RT).[6,7] Integration of functional PET data with anatomic CT data should be a standard in RTP.[3] It remains a challenge, however, to quantify the improvement of simulation with PET/CT over CT in RTP because conclusive clinical data are not yet available. Early studies have found PET/CT has advantages over CT and MR imaging in the standardization of volume delineation,[8–11] in the reduction of the risk for geometric misses,[12] and in the minimization of radiation dose to the nontarget organs.[2,4,13] Utilization of PET/CT for RTP is expected to grow as more molecular targeted imaging agents are developed. Today, there are more than 2000 PubMed entries that result from a search using "PET" AND "Radiotherapy" (**Fig. 1**).

There are several challenges in PET/CT imaging for RTP. The first one is lack of reimbursement for PET/CT simulation. In the United States, each cancer patient is reimbursable for only one PET/CT scan before treatment, which may include surgery, chemotherapy, and radiation therapy (RT). This PET/CT scan is normally for diagnosis/staging. There are no data to support PET/CT simulation for NSCLC, esophageal, and head and neck patients, who are likely to benefit from PET/CT simulation. Most patients have their diseases characterized with the help of PET/CT before RT, and there is no reimbursement for PET/CT simulation for RT. This has significantly limited the application of PET/CT simulation for RT.

Patient setup and scan coverage are different between PET/CT imaging for diagnosis/staging and PET/CT imaging for RTP. The majority of PET/CT scans are performed in settings for disease diagnosis and patient management. It is typical to scan from the orbit to the midthigh for diagnosis/staging. The exception is head-to-toe coverage for melanoma cancer patients. The total time for scanning a patient is approximately 30 minutes, including patient setup time. Patient comfort and throughput are critical for the clinical operation. If PET/CT is used for RT, an immobilization device for the patient at treatment position should be made before fludeoxyglucose F 18 (^{18}F-FDG) injection to reduce the radiation exposure to the staff. After positioning the patient at the treatment

This work was supported by grant No. SNSF 31003A-125246 from the Swiss National Foundation and Geneva Cancer League.

[a] Division of Nuclear Medicine and Molecular Imaging, Geneva University Hospital, CH-1211 Geneva, Switzerland
[b] Geneva Neuroscience Center, Geneva University, CH-1211 Geneva, Switzerland
[c] Department of Imaging Physics, MD Anderson Cancer Center The University of Texas, Houston, TX 77030, USA
* Corresponding author. Division of Nuclear Medicine and Molecular Imaging, Geneva University Hospital, CH-1211 Geneva, Switzerland.
E-mail address: habib.zaidi@hcuge.ch

PET Clin 6 (2011) 207–226
doi:10.1016/j.cpet.2011.02.009

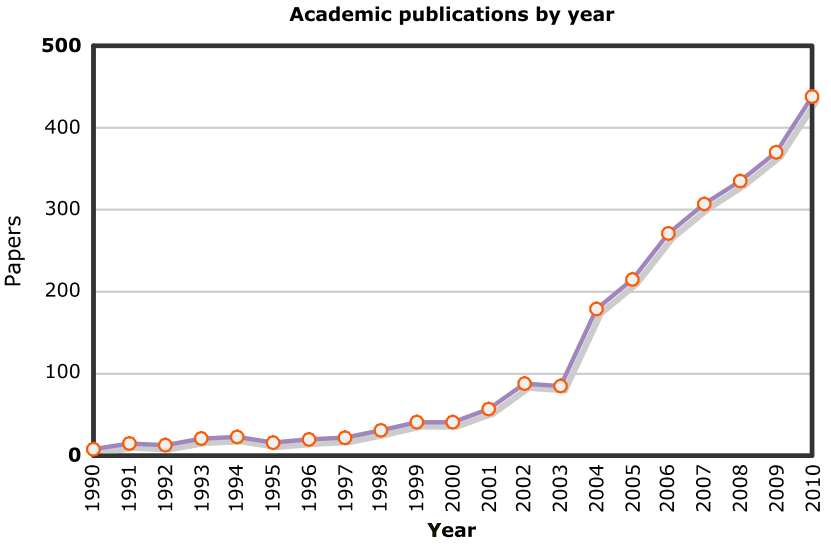

Fig. 1. The increasing number of annual peer-reviewed publications reporting on the use of PET and PET/CT in RT demonstrates the growing interest in PET-guided treatment planning. This graph is based on a PubMed query using the following MeSH terms: "RADIOTHERAPY" OR "RADIATION THERAPY" AND "POSITRON EMISSION TOMOGRAPHY". A timeline was created with MEDSUM, an online MEDLINE summary tool by MJ Galsworthy. Hosted by the Institute of Biomedical Informatics, Faculty of Medicine, University of Ljubljana, Slovenia (www.medsum.info.)

position, the disease area is scanned, such as the thorax for NSCLC and the head and the upper torso for head and neck cancer, unless the progression of the disease has changed after the diagnosis. Current PET/CT simulation procedures are mostly performed for the assessment of treatment response when RT is considered as a part of the treatment. If a limited coverage, such as the thorax or the head and neck area, can be prescribed for PET/CT simulation for RT, just like the current CT simulation for RT, the floodgate of PET/CT for RT will be opened. The continuing adoption of PET/CT to cover many disease indications and the continuing decline of reimbursement coupled with the drop of the PET/CT scanner are likely to open this floodgate in the future.

There are many factors that could affect the accuracy of quantification with PET/CT imaging for RT.[14] The most challenging one has been with imaging of the thoracic tumor or the NSCLC, in which respiratory motion could have an impact the diagnostic and staging accuracy. This review documents the recent technical advances in the field with special emphasis on the conceptual role of molecular PET/CT imaging RTP and the challenges arising from technical and physiologic factors that still need to be addressed. Much worthwhile research and development efforts remain to be done and many of the techniques reviewed are themselves not yet widely implemented in clinical settings.

NOVEL TRACERS AND TUMOR HYPOXIA

Recent advances in the development of novel tracers targeted to other aspects of tumor biology, including cell growth, cell death, oncogene expression, drug delivery, and tumor hypoxia, will significantly enhance the capability of clinical scientists to differentiate tumors and are likely to be used to guide treatment decisions. Several new tracers are expected to be approved and routinely used in the coming years.[15] The list of new tracers having the potential for routine use in the near future is long and not reviewed in this article. Interested readers may consult recently published reviews addressing this topic.[16–19] In certain cancers, ^{18}F-labeled fluorothymidine may prove to be of value in monitoring response to therapy instead of ^{18}F-FDG.[16] This tracer, however, does not seem optimal for diagnostic purposes because it is insensitive for detecting slow-growing tumors. ^{18}F-labeled DOPA[17] along with ^{68}Ga-labeled DOTA octreotide[18] and ^{124}I-metaiodobenzylguanidine[19] seem to have the promise of improving the management of patients with neuroendocrine tumors. Peptides containing amino acid sequence arginine-glycine-aspartate (RGD) seem to have an affinity toward integrins that are present on activated endothelial cells in tumors with angiogenesis.[20] ^{18}F-Galacto-RGD is a tracer developed for specific imaging of $\alpha_v\beta_3$ expression, a receptor

involved in angiogenesis and metastasis that proved particularly useful in patients with squamous cell carcinoma of the head and neck.[21] Estrogen receptor targeting agents may be used to assess noninvasively the estrogen receptor section of tumors in vivo by ^{18}F-labeled estrogen analogues, such as fluoestradiol.[22] Angiogenesis, the formation of new vessels, is the target of a multitude of novel therapies and drugs. Therefore, direct visualization of this biologic response to tumor hypoxia and cell proliferation will be of great importance in developing these drugs. Peptides containing amino acid sequence RGD seem to have an affinity toward integrins that are present on activated endothelial cells in tumors with angiogenesis.[20] Apoptosis or programmed cell death can be imaged with radiolabeled Annex V to monitor response to therapy in cancer.[23]

Agents that measure regional hypoxia in malignant tumors (eg, FMISO, ^{18}F-EF5, and ^{64}Cu-ATSM) and possibly in some benign disorders will be frequently used,[24] especially in the context of RTP.[25] Tissue hypoxia is a pathologic condition in which a region of the body is deprived of adequate oxygen supply and is a major constraint for tumor treatment by RT. The efficacy of ionizing radiation directly relies on adequate supply of oxygen to the targeted tumor. As a tumor grows, it needs oxygen in order to survive. Although the tumor develops new blood vessels by a process of angiogenesis, these new vessels are typically less extensive than in normal tissues. As a result, the tumor cells do not receive adequate oxygen from the blood, leading to hypoxia and leaving portions of the tumor with regions where the oxygen concentration is significantly lower than in healthy tissues. Hypoxic tumor cells are usually resistant to RT and chemotherapy, but they can be made more susceptible to treatment by increasing the amount of oxygen in them. Furthermore, hypoxia is related to malignant progression, increased invasion, angiogenesis, and an increased risk of metastases formation.[26] There are three distinct types of tumor hypoxia[27]: (1) perfusion-related (acute) hypoxia, which results from inadequate blood flow in tumors; it is generally the consequence of recognized structural and functional abnormalities of the tumor neovasculature; (2) diffusion-related (chronic) hypoxia caused by increased oxygen diffusion distances due to tumor expansion; and (3) anemic hypoxia related to the reduced oxygen-carrying capacity of the blood.

Two different strategies can be used to overcome the problem of hypoxia-mediated radioresistance. The first strategy is to improve the tumor oxygenation during RT. The second strategy is to target hypoxia as a relatively unique feature of tumor tissue by means of drugs, which are activated under hypoxic conditions and act as hypoxic radiosensitizers or hypoxic cytotoxins.[26]

^{18}F-MISO and Cu-ATSM are the most widely used tracers in PET for their ability to demonstrate heterogeneity and general availability.[28] ^{18}F-MISO has relatively slow blood clearance and high lipophilicity contributing to significant background activity and relatively low contrast between hypoxic and normal tissues.[29] One remedy to this was to acquire a venous blood sample during the course of the imaging procedure for a tumor-to-blood ratio image to improve the contrast. ^{18}F-MISO is able to monitor the changing hypoxia status of lung tumors during RT.[30] Studies in sarcoma[31] and head and neck cancer[31,32] have demonstrated a correlation of ^{18}F-MISO uptake with poor outcome to radiation and chemotherapy.

Cu-ATSM is another promising agent for delineating the extent of hypoxia within tumors. Most Cu-ATSM studies have used the short-lived copper Cobalt-60 (^{60}Cu) (half-life of 0.395 hours), which requires an on-site cyclotron. One advantage of using shorter-lived ^{60}Cu is the ability to perform multiple imaging sessions in a short time frame. To enable the transport of Cu-ATSM to the PET facilities without a cyclotron, longer-lived ^{61}Cu (half-life of 3.408 hours) and ^{64}Cu (half-life of 12.7 hours) are alternatives. Many preclinical studies have validated its use for imaging of hypoxia in tumors and other tissues. One concern with using Cu-ATSM to delineate hypoxia was that it may be tumor dependent, and cell-line dependent. It was demonstrated that there was variation in the ^{64}Cu-ATSM cellular accumulation, with uptake in normoxic cells being anywhere from 2 to 9 times lower than that in hypoxic cells, depending on the cell line. Nonetheless, ^{64}Cu-ATSM has been shown highly correlated with ^{18}F-FMISO in an animal model.[33] In human studies of lung[34] and cervical cancers,[35,36] ^{60}Cu-ATSM can act as a prognostic indicator for response to therapy. In a prospective study of 14 patients with NSCLC, a semiquantitative analysis of the ^{60}Cu-ATSM tumor-to-muscle ratio was able to discriminate those likely to respond to therapy from nonresponders.[37] A similar study in 14 women with cervical cancer demonstrated a similar predictive value in the tumor response to therapy. In the same study, tumor ^{18}F-FDG uptake did not correlate with ^{60}Cu-ATSM and there was no significant difference in tumor ^{18}F-FDG uptake between patients with hypoxic tumors and those with normoxic tumors.[37] ^{18}F-EF5 is another

promising agent,[38,39] which proved useful for noninvasive clinical assessment of hypoxia in brain tumors.[40]

PET/CT-GUIDED RADIATION THERAPY

Early attempts to use nuclear medicine imaging, in particular PET, for RTP date back to the late 1990s.[41–48] An important contribution came from Ling and colleagues.[49] who established the concept of biologic imaging and moved forward the role of PET in RT, thus allowing it to enter the clinical arena. Since that time, the technical aspects of PET/CT-guided RT have been described more thoroughly in the scientific literature.[3,7,41–45,50–52] The success of these initial studies prompted significant interest from the major medical imaging equipment manufacturers, who all have introduced commercial PET/CT scanners equipped with the required accessories (flat couch insert, positioning system, respiratory gating, and other accessories) and software tools (virtual simulation, visualization and segmentation tools, support of Digital Imaging Communication in Medicine (DICOM) RT object definition, and other tools) for clinical use.[46] The typical workflow for PET/CT-guided RTP, usually involving two clinical departments (nuclear medicine and radiation oncology), is shown in **Fig. 2**.[7,47] With the growing availability of large-bore dual-modality PET/CT scanners equipped with fixed RT positioning laser systems in the scanner room, a one-stop shop providing diagnostic PET/CT and RTP CT scan in only one session has become possible.[7]

The main motivation stimulating the use of PET/CT in RT is the efficacy of ^{18}F-FDG–PET imaging in a wide variety of malignant tumors with sensitivities, specificities, and accuracy often in the high 90th-percentile range.[48] In that sense, it might provide superior visualization compared with CT simulation, which in some cases might miss some areas that light up on the PET study, including the detection of distant metastases, or shed the light on the actual lesion volume, which might in reality be smaller on the PET study than on the CT alone. Moreover, discrepancies between anatomic (CT/MR imaging) and metabolic (PET) findings are often reported in the literature where the addition of PET has a significant impact on patient management and changed the treatment plans in 25% to 50% of cases.[1,3,5,53–61] Last and not least, interobserver and intraobserver variability was considerably reduced when PET information was available for target volume delineation.[8,62–65] Both state-of-the-art ^{18}F-FDG-PET and novel PET probes applications in the process of RTP are discussed elsewhere[7,66–68] and are beyond the scope of this review.

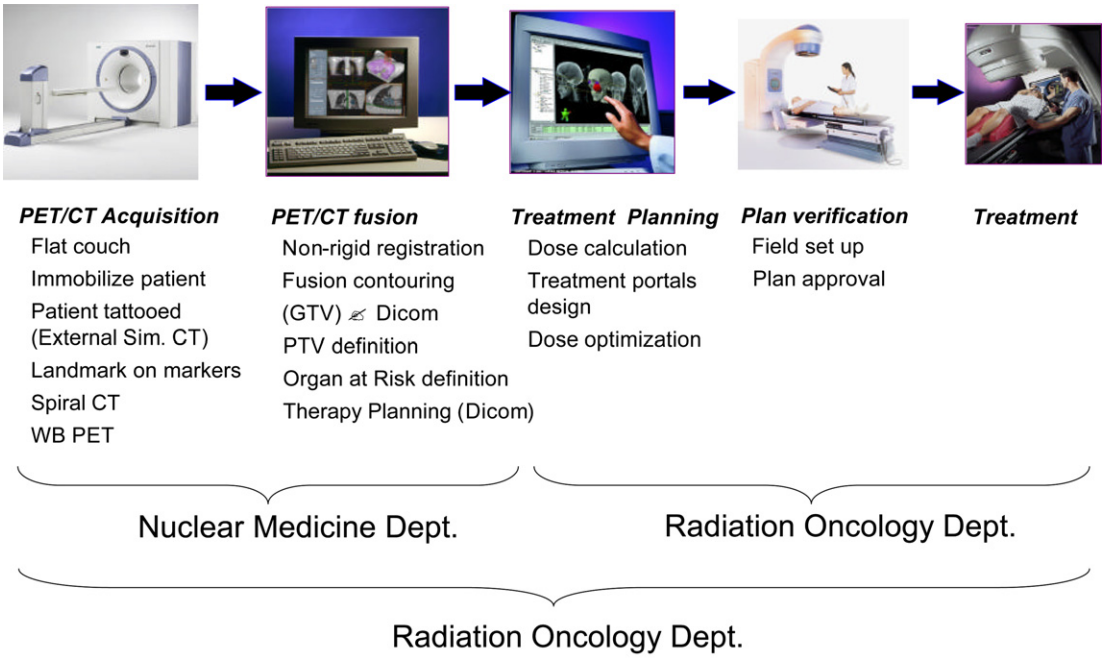

Fig. 2. Typical workflow for PET/CT-guided RTP where usually two clinical departments are involved (nuclear medicine and radiation oncology). Many academic radiation oncology facilities are now equipped with combined PET/CT scanners, which allows them to operate in complete autonomy.

Current indications for ^{18}F-FDG–PET/CT-guided RTP fall in two classes: established and experimental. Well-established indications include head and neck cancer, lung cancer, gynecologic cancer, and esophageal cancer whereas experimental indications comprise colorectal cancer, breast cancer, lymphoma and malignant melanoma, and many other malignancies.[7]

CHALLENGES OF PET/CT-GUIDED RADIATION THERAPY

Respiratory Motion

Misregistration between the CT and PET data due to the respiratory motion in the thorax and abdomen was reported soon after commercial PET/CT was introduced in 2001[53,69–72] and has been one of the most researched topics in PET/CT. Fast gantry rotation of less than 1 second per revolution and a large detector coverage of greater than 2 cm enable a CT scan of more than 100 cm in the cranial-caudal direction in 20 seconds. Alternatively, it normally takes 2 to 5 minutes to acquire the PET data of every 15 cm.[54,73] The temporal resolutions of CT and PET are different: less than 1 second for CT and approximately 1 respiratory cycle for PET. This mismatch in the temporal resolution may cause a misalignment of the tumor position between the CT and the PET data and may compromise quantification of the PET data.[66] The current design of PET/CT only matches the spatial resolutions of the CT and PET data by blurring the CT images so that the spatial resolution of the CT images matches the spatial resolution of the PET images. There has been no attempt from the manufacturers to match the temporal resolutions of CT and PET for a routine whole-body PET/CT scan.

Mismatch between the CT and PET data can be identified by a curvilinear white band or photopenic region at the diaphragm in the PET images. Existence of the white band only suggests a misregistration at the diaphragm. It is possible to have either a good registration or misregistration at the tumor location with or without a white band at the diaphragm. Because time is spent exhaling than inhaling, the PET data averaged over several minutes is closer to the end-exhale than the end-inhale. If the CT data are acquired near the end-exhale, then there is a good registration between the CT and the PET data. Alternatively, if the CT data are acquired in or near the end-inhale, the inflated lungs of inhale are larger than the deflated lungs of exhale. The larger area of the inflated lungs in CT renders less attenuation correction in the reconstruction of the PET data near the diaphragm where the inflated lungs push the diaphragm lower in CT than the average diaphragm position in PET. The result is a white band region identified as the misregistered region or the photopenic region.

The rate of misregistration can be as high as 68%[67] to 84%.[70] It only has an impact on 2% of the diagnosis in a whole-body PET/CT with ^{18}F-FDG[74] and could be false positive in 40% of the cardiac PET/CT studies with Rubidium-82.[75] In the whole-body PET/CT for oncology, many lesions may not be close to the diaphragm where most misregistrations occur, and the task of diagnosis is generally not compromised by a misregistration between the CT and the PET data. Because the heart is right above the diaphragm, and the diagnosis of a cardiac PET is dependent on an accurate quantification of the PET data, a more stringent requirement in registration is needed for the cardiac PET/CT than for the whole-body PET/CT. For RT, a study of 216 patients in quantification with standardized uptake value (SUV) and gross target volume (GTV) delineation[67] indicated that 10% of the misregistrations could cause an SUV change of more than 25%, a threshold indicating a response to therapy,[76] and tumors of size less than 50 cm^3 near the diaphragm could have a change of the centroid tumor location of 2.4 mm, a GTV change of 154%, and an SUV change of 21%. More data are warranted to assess the impact of misregistration on RT.

Fast translation of the CT table during a helical CT scan may not eliminate or reduce misregistration between the CT and PET data. The CT images register better between slices if the CT scanner has at least 6 slices.[73] As long as the CT scan is conducted when the patient is free breathing, there are always some CT slices taken at inhale and some at exhale. The distance between the inhale and the exhale can become longer (or shorter) with a faster (or slower) speed helical CT scan. Fast CT gantry rotation can help freeze the motion and reduce motion artifacts in each CT slice and subsequently improves the PET image reconstruction. There is a difference between motion artifacts in each CT slice and registration of the CT images between slices. A fast gantry rotation speed can help reduce the motion artifacts in each CT slice. A faster helical CT scan with a higher pitch and a faster gantry rotation speed can help improve the registration between the CT slices. None of these can fix the problem of misregistration between the CT and PET data. **Fig. 3** shows an example of a whole-body helical CT scan in PET/CT with a 16-slice CT. There were respiratory artifacts on the abdomen and cardiac pulsation artifacts on the heart, which

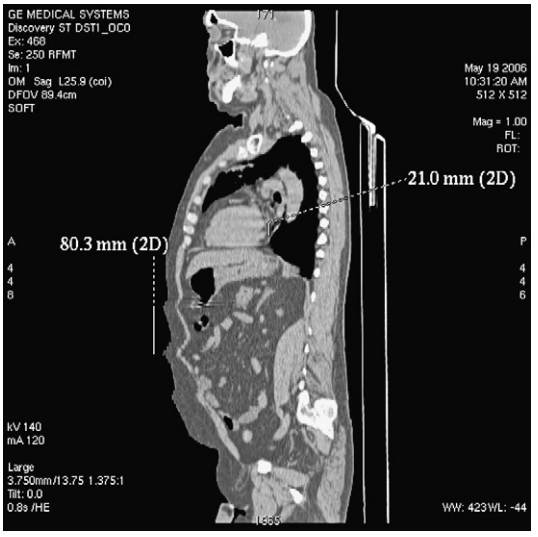

Fig. 3. An example of deriving the breathing cycle and heart rate from the motion artifacts in a free-breathing helical CT. There were breathing and cardiac pulsation artifacts on the abdomen and the heart in a free-breathing helical CT scan of pitch 1.375 to 1, x-ray collimation of 1 cm, and gantry rotation cycle of 0.8 second. The measured distances of periodicity were 80.3 mm and 21.0 mm for the breathing and cardiac pulsation artifacts, respectively. The speed of the helical CT scan was 17.2 m/s. The breathing cycle and the heart rate were estimated to be 4.67 seconds and 49 beats per minute.

were not discernible in the review of each individual CT slice. By measuring the distance between the adjacent peaks of the respiratory (cardiac pulsation) artifacts and dividing the distance to the table translation speed of the helical CT scan, the breathing cycle (the heat rate) of the patient can be estimated. These artifacts were due to the respiration and heart beating of the patient and are always with patient data. The presentation of the artifacts depends on the speed of the helical CT scan, however, and the breathing patterns of a patient during the helical CT scan.

Coaching patients to hold breath in the middle of exhale during the CT acquisition was suggested as a way to improve the registration of the CT and the PET data,[55] and the outcomes were mixed due to an unreliable coordination between patient and technologist. First, the definition of midexhale is subjective to patients. Breath hold at midexhale can mean midexhale in either a light or deep breathing. When a patient is asked to hold breath, there is a tendency for the patient to want to breathe in more air to maintain the subsequent midexhale breath hold. Second, a technologist has to give the breathing instruction and scan the patient at the same time, adding to the complexity of operation. An example is shown in **Fig. 4**. More than 50% of the PET/CT data in a study of midexhale breath holds were with a white band at the diaphragm.[66] Today most clinics are scanning patients without any breathing instruction. In many cases, the registration between the CT and PET data for a patient in light breathing is often better than the one with coaching the patient to breath hold at the midexhale position.

One approach of improving the registration between the CT and the PET data is to bring the temporal resolution of the CT images to that of the PET data.[66] Because PET is averaged over many breath cycles, an average CT over 1 breath cycle helps improve the registration between the CT and the PET data. In this technique, the average CT data are acquired at a very high gantry rotation speed over 1 respiratory cycle. A scan of 4 seconds allows for 8 gantry rotations of 0.5 seconds. This is to ensure that each projection angle can collect as many phases of data as possible to allow data averaging over 1 respiratory cycle. Ideally, averaging the many projections or phases of the respiratory motion can be performed before image reconstruction. Current CT scanners do not have this function. Instead, multiple CT images of high temporal resolution are reconstructed and averaged for an average CT.[56] This is different from the slow CT scan technique with a slow gantry rotation of 4 seconds for an average CT, suggested by the American Association of Physicists in Medicine Task Group 76 for imaging the lung tumors not involved with either the mediastinum or the chest wall and not for the tumor of the liver, pancreas, and kidney.[57] A cine CT scan for average CT acquires consistent data in a fast CT rotation, and the object does not change its position much during a fast CT rotation. Alternatively, a slow scan CT acquires inconsistent data over a slow CT scan, producing the images with severe reconstruction artifacts due to the motion. A patient study is shown in **Fig. 5** to illustrate the difference in image quality between the average CT and slow scan CT at the diaphragm.

In terms of temporal resolution, average CT is similar to the transmission map acquired with 2 to 3 rotating transmission rod sources of Germanium-68 for attenuation correction of the PET data, shown to have an excellent registration with the emission PET data.[77,78] The advantages of cine CT averaging over transmission rod sources are (1) short acquisition time: 1 minute for cine CT and 10 minutes per 15 cm in transmission and (2) high photon flux and less noisy attenuation maps. The disadvantage is higher radiation dose (<0.83 mSv for the average CT acquired with

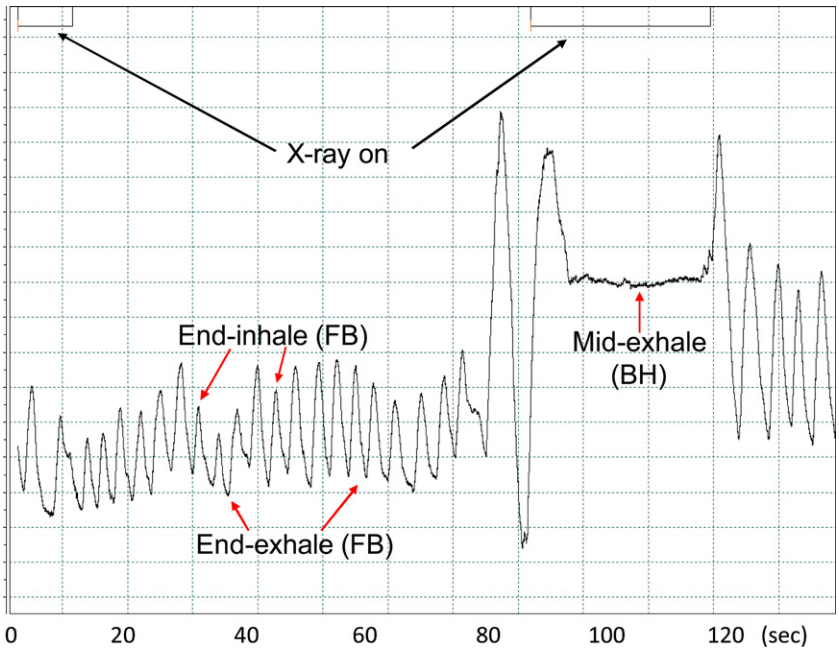

Fig. 4. A breathing trace of a patient during a helical CT scan. The two places of x-ray on are shown for the scout and helical CT scans. The patient was free breathing until a breathing instruction was given as "breath in, breath out," and hold your breath at midexhale. The difference between the breath-hold state and the free-breathing state caused a misalignment between the CT and the PET data. (*Reproduced from* Pan T, Mawlawi O, Nehmeh SA, et al. Attenuation correction of PET images with respiration-averaged CT images in PET/CT. J Nucl Med 2005;46:1481–87; with permission.)

10 mA for 5 s or 50 mAs and I<10 cm scanning) compared to approximately 0.13 mSv for the transmission rod sources.[79] Average CT can be sensitive to an irregular respiratory cycle during the data collection. One remedy for this is to acquire 2 respiratory cycles per table position so that an irregular respiratory cycle can be removed if needed. **Fig. 6** shows an example. By removing the irregularity, a normal average CT data can be obtained. RT has embraced the use of average CT for dose calculation,[58] in particular for proton beam therapy.[59] It has been shown that the average CT derived from cine CT is equivalent to the average CT from 4-D CT as far as dose calculation.[58] Because most of the new PET/CT scanners are not equipped with transmission rod sources, average CT cans serve as an alternative with the additional benefits in dose calculation for RT. **Fig. 7** shows an example of misregistration between the CT and the PET data and correction of misregistration by average CT to improve the accuracy of quantification for diagnosis. **Fig. 8** shows another example of misregistration that caused a false-negative diagnosis and a change of the location of the GTV for RT. In the era of image-guided RT, when RT can deliver a very high dose at great precision, it is important to pay attention to any misregistration between the PET and the CT images during tumor delineation.

Average CT was first proposed for tumor imaging[66] and subsequently for cardiac imaging.[56] Its effectiveness was confirmed by other researchers[80,81] and in several clinical studies.[82–85] Although cine CT is associated with high radiation exposure for its long acquisition time, it should be applied judicially to the area of the targeted tumor with a radiation exposure of less than 5 mGy for diagnosis and less than 50 mGy for RT.[56] In comparison, the exposure of a typical diagnostic CT scan is approximately 20 mGy or higher. One way of minimizing the radiation dose is to apply average CT when there is a misregistration identified in the thorax or abdomen. In a typical PET/CT scan, the thorax and the abdomen images are available for review before the completion of the scan, and a decision to acquire average CT can be made accordingly. In RT, the amount of radiation is not a major concern due to the therapy dose of up to 70 Gy.

A novel technique to image patients at deep-inspiration breath hold (DIBH) for accurate quantification was first suggested by Nehmeh and colleagues[60] and has gained attention by several researchers.[61–65,68] Patients are asked to hold

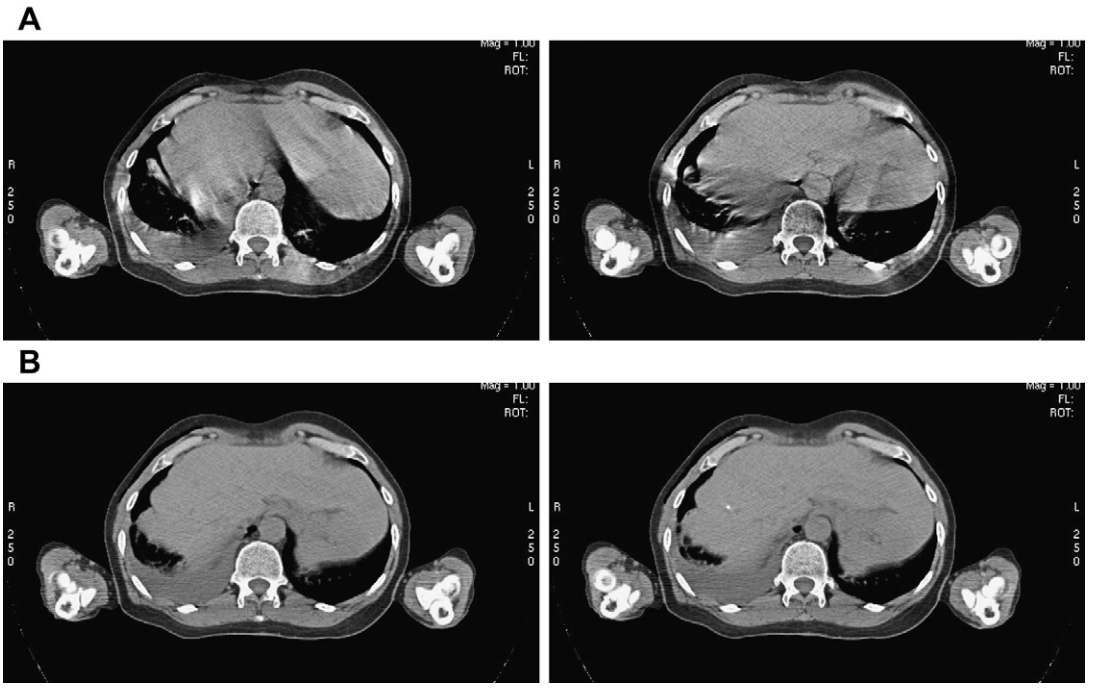

Fig. 5. The average CT (ACT) and the slow scan CT (SSCT) images of a patient with an average breath cycle of 4 seconds. The SSCT images (*A*) were taken with one single CT gantry rotation of 4 seconds, and the two images were taken with two separate acquisitions 2.5-mm apart and 2.5-mm thick. The corresponding ACT images (*B*), obtained by averaging the cine CT images, were averaged from 4 seconds of data collection over 8 gantry rotations. The ACT images were almost free of the reconstruction artifacts, evident in the SSCT images. (*Reproduced from* Pan T, Mawlawi O, Luo D, et al. Attenuation correction of PET cardiac data with low-dose average CT in PET/CT. Med Phys 2006;33:3931–8; with permission.)

breath at deep inspiration during CT and PET acquisition so that the tumor can be maintained stationary during the data acquisition. One study suggested a single DIBH of 20 seconds[63] and most studies used multiple DIBHs to improve the statistics of the PET data. There were some issues related to this technique: (1) applicability to the lung cancer patients with a compromised lung function, (2) potential mismatch between the CT and the PET data at DIBH, (3) reproducibility of the multiple DIBHs during the PET data acquisition, and (4) higher SUV due to the noisy PET data acquired in a duration of 1 or multiple breath holds. Some clinical data have suggested improvement in quantification and registration of the CT and the PET data with this technique. Because most of the RT procedures are conducted under normal breathing, this approach may be more applicable to staging and treatment response assessment than to RT simulation.

Respiratory gating is another important development in PET/CT for RT. In an evaluation of patients scanned in the past 6 years with a dedicated PET/CT scanner for RT in the University of Texas MD Anderson Cancer Center, Houston, Texas, there were more than 4000 patients simulated with 4-D CT[77,86] and only 700 patients with PET/CT. In terms of demographics, all thoracic RT patients for lung, esophageal, or liver disease were 4-D CT simulated. Iodinated contrast media was incorporated in 4-D CT imaging of the liver tumor to enhance the contrast between the liver tumor and the parenchyma for treatment planning.[74] For the 700 PET/CT scans, there were 63% for non–small cell lung cancer (NSCLC), 14% for esophageal cancer, 13% for head and neck cancer, 1% for solitary pulmonary nodules, and 9% for the other indications. The PET/CT scans for RT were performed when staging was requested and RT was included in the treatment. The number of PET/CT scans performed on this scanner was limited because there was only one PET/CT scan reimbursed per patient before treatment, and the PET/CT scan is normally conducted for the purpose of diagnosis, not for RT. In total, there were 64% of the 700 PET/CT scans (NSCLC and solitary pulmonary nodules) of lung cancer. This is in contrast to an average of 32% PET/CT procedures performed for the lung cancer in general.[87] If the esophageal cancer patients are

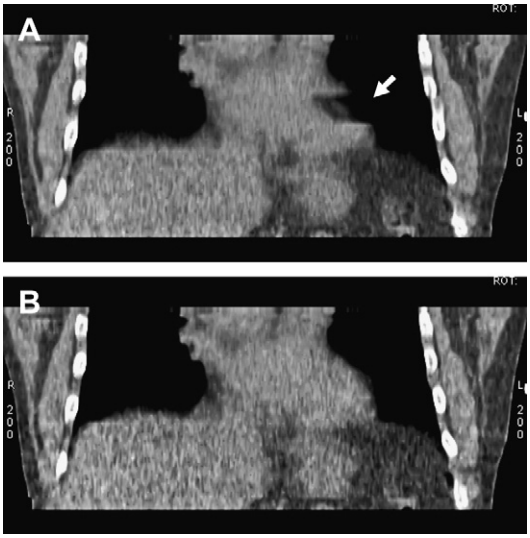

Fig. 6. (*A*) The average CT image from a cine acquisition of 10 seconds, which is approximately 2 respiratory cycles, and (*B*) the average CT image from 5 seconds or 50% of the 10-second cine CT data after removing an irregular respiratory cycle of data pointed by an arrow (*A*). This example demonstrated the importance of regular respiration in the cine CT acquisition and the potential of removing an irregularity to derive a normal average CT if there is more than 1 respiratory cycle of data to choose from.

included, there were almost 78% of the RT PET/CT patients for whom the tumor motion from respiration was assessed with 4-D CT in a single session of PET/CT simulation. The PET data were attenuation corrected with average CT from the cine CT data in 4-D CT to improve the registration of the CT and the PET data.

Although 4-D PET[88] can also be performed on this PET/CT for RT, its application has been limited due to the total acquisition time approaching 40 minutes.[89] Most patients cannot hold their arms up over their heads for more than 30 minutes and the long acquisition time could induce patient motion and compromise the PET/CT study. Moreover, the statistics of 4-D PET is poor due to splitting up the coincidence events into multiple bins or phases for 4-D PET, and the spatial resolution of PET in general is only approximately 5 to 10 mm.[90] In a recent clinical investigation of 18 patients with 4-D PET,[89] it was found that respiratory gating increases SUV by 22.4% and improves the consistency of tumor volumes between PET and CT. This study was the first clinical investigation reported since the introduction of 4-D PET/CT in 2004.[91] In contrast, 4-D CT can be performed in less than 2 minutes for the coverage of the whole lungs. There is normally high contrast between the lung tumor and the parenchyma except when the lung tumor is connected to a similar tissue density of the mediastinum and chest wall. It is relatively easy to incorporate 4-D CT than 4-D PET in a PET/CT simulation.

List-mode data acquisition,[92] extension of axial field of view,[93] and time-of-flight[82] technologies could in the future catapult 4-D PET into a routine clinical procedure. Today many PET/CT scanners can acquire the list-mode PET data to reconstruct a static PET data set as in a routine PET scan. The same list-mode data can also be reconstructed for the gated PET data if the corresponding respiratory signal were recorded during data acquisition. The advantage of this approach is that the static data can be used as a part of the gated data to offset the long acquisition time for 4-D PET. Increasing the axial field of view from 15 to 22 cm can increase the sensitivity of data acquisition and shorten the scan time of 4-D PET. The time-of-flight technology, which helps localize more accurately each coincidence event in the image space than the conventional PET without time of flight, can improve the signal-to-noise ratio and reduce the scan time of 4-D PET.[82] Integration of the new technologies in a clinic environment with an efficient image reconstruction process and a simple workflow are critical for 4-D PET to be clinically feasible.

Partial Volume Effect

Partial volume effect (PVE) is the underestimation of activity concentration in a lesion due to the limited spatial resolution of PET, which is in the range of 5 to 10 mm for clinical PET/CT systems. PVE has an impact on most quantification of small lesions of size less than 2 to 3 times the PET spatial resolution.[83,94] Any factor contributing to image reconstruction, image filtering, and presentation of images also has an impact on PVE. It is also related to the metric used to measure the activity concentration, such as the maximum activity concentration of a voxel or the average activity concentration of a volume in a tumor. The most used metric is the maximum SUV, which is sensitive to the noise but not dependent on the selection of a volume as is in the average activity concentration. In general, a tumor of size less than 3 cm look larger but less aggressive than it actually is in PET.[83,94] Although it has been 30 years since PVE was researched and attempted for correction,[95] correction of PVE in PET imaging is not yet clinically available.

Several approaches have been proposed to compensate for the PVE[83] with many of them developed specifically for brain imaging.[94] These can

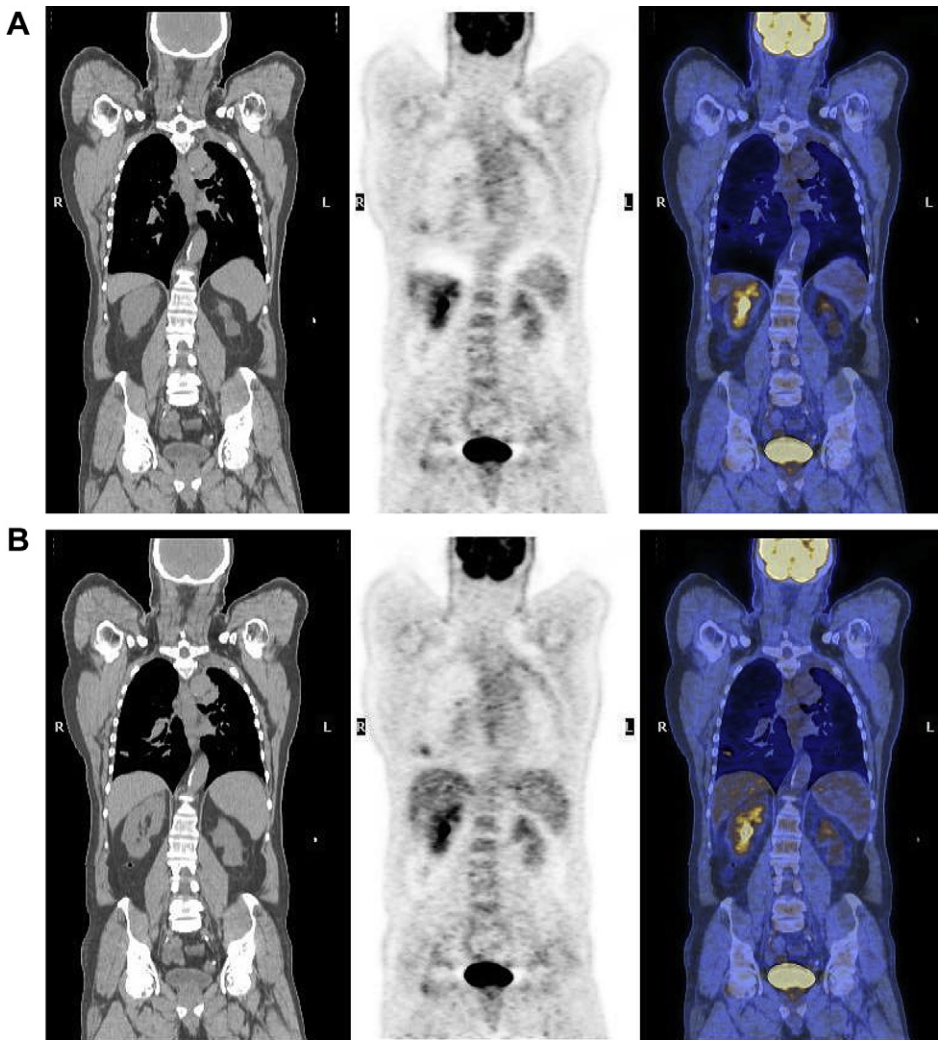

Fig. 7. The CT, PET, and fused PET/CT images of an NSCLC patient with misregistration near the diaphragm are shown (*A*), and the corresponding images with attenuation correction with the average CT data are shown (*B*). The maximum SUV increased 57% from 2.3 (*A*) to 3.6 (*B*). In this comparison, the same PET data were reconstructed with the conventional CT (*A*) and average CT (*B*).

broadly be divided into (1) postreconstruction-based methods and (2) reconstruction-based methods. Each of these two categories can be implemented in the form of either region of interest (ROI)-based or voxel-based approaches. Potential advantages of PVE-corrected images, as opposed to PVE-corrected ROI-measured concentrations, include the capability to accurately outline functional volumes as well as improving tumor-to-background ratio, which could considerably improve diagnostic examinations, studies involving the assessment of response to treatment, and PET-based RTP. In this context, however, the problem is more complex and relies in many cases on a number of often-strong assumptions and approximations.[94]

Recovery coefficient (RC) is a simple method of estimating the true quantitative value if the tumor of interest has a size and shape similar to the ones already modeled through simulation or measurement.[95] It can be implemented with a look-up table and can be computationally efficient. For a spherical tumor, the RC can be derived as a function of the sphere size and the signal-to-background ratio (SBR) for a wide range of spatial resolution values.[96] A simple correction can be performed by dividing the measured activity with the RC corresponding to the size and shape of the metabolically active tumor. Homogeneous activity concentration and simple geometry tumors are easier for the correction with RC than the inhomogeneous activity concentration and

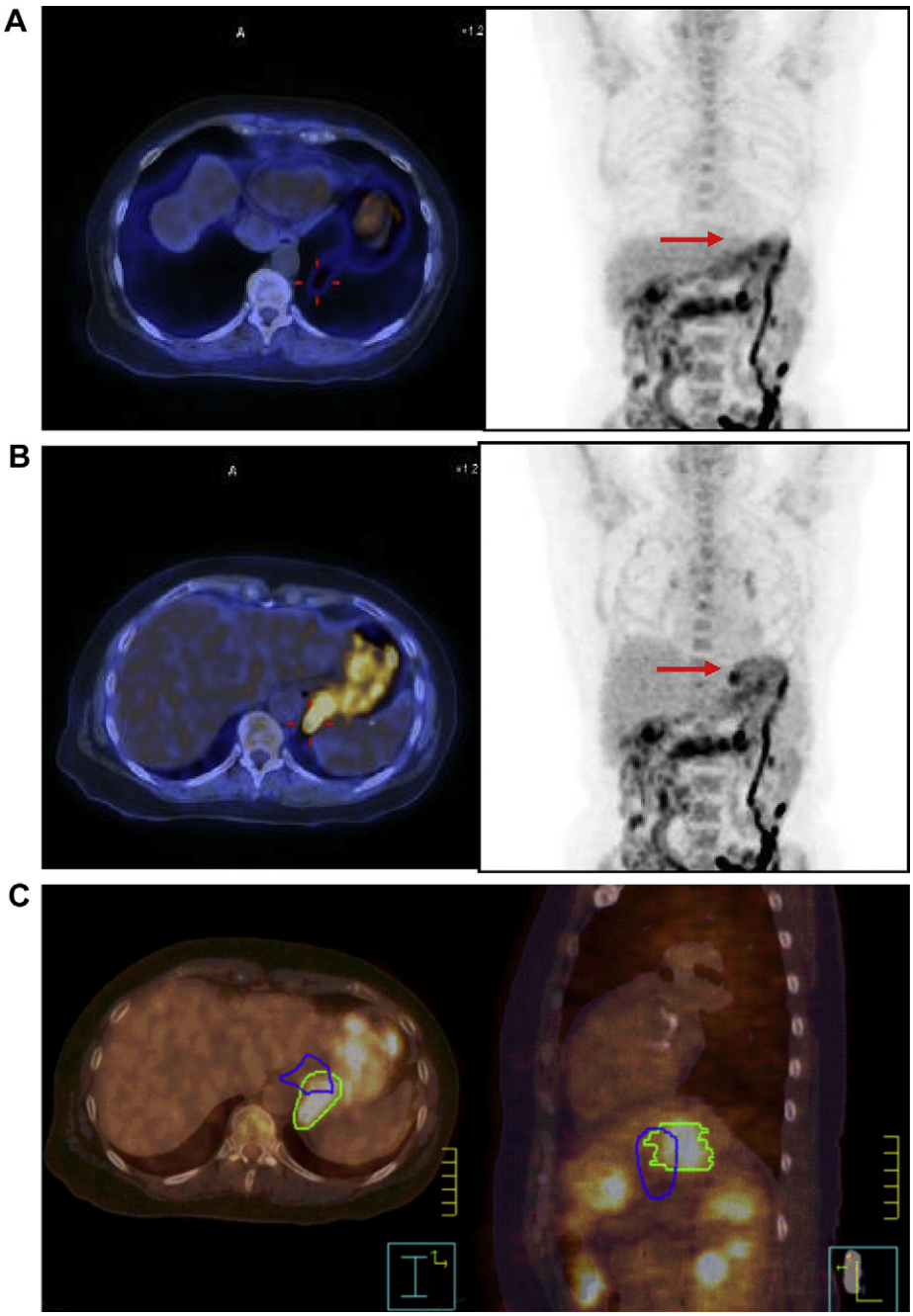

Fig. 8. The PET/CT images of a 69-year-old female patient with an esophageal tumor after induction chemotherapy. (*A*) Shows an axial slice of the fused clinical CT and PET image at the level of the esophageal tumor (*left*) and the PET image in coronal view (*right*). The radiology report indicated the patient had a positive response to the chemotherapy. After removal of misalignment by the average CT, the tumor reappeared in the same PET data set (*B*). The arrows point to the tumor location. The GTVs drawn in the images (*A*) and (*B*) are shown in blue and in green, respectively (*C*). The patient was treated with the tumor volume in green, and the radiology report was corrected by the average CT. (*Reproduced from* Pan T, Mawlawi O. PET/CT in radiation oncology. Med Phys 2008;35:4955–66; with permission.)

irregular geometry tumors. In this early publication, the PVE was tackled in the framework of hot objects in a cold background, thus addressing only one aspect of the problem, referred to as spill-out (loss of activity owing to the small size of the object relative to the PET scanner's spatial resolution). It was also realized that, depending on the background's activity concentration, spill-in from the surrounding warm tissues might be as important as spill-out and should be compensated.[94] The concept of contrast RC was introduced[96] to reflect the rate of recovery that lies above the surrounding medium. This quantity is only justified when the background is not itself subject to PVE and is of known and uniform activity concentration. The method is commonly used in oncologic PET imaging where a priori information about the tumor size and shape can be made available.[78–80,97–99] The approach is limited, however, by the crude approximations involved and more sophisticated techniques were sought.

A more sophisticated approach is to enhance the PET resolution by modeling the detector response into the system matrix in iterative image reconstruction[81,84] because reconstruction methods that improve the effective spatial resolution of the scanner can compensate for PVE. In this sense, there are many approaches to reconstruction that attempt to achieve the aforementioned goals[85,100]; the use of statistical iterative reconstructions has been an important step in this direction both for voxel-based[101,102] and ROI-based[103–106] reconstructions. Incorporation of the anatomic information from MR imaging in the reconstruction has been proposed for brain imaging[107] and might in the future be extended to other applications with the introduction of dual-modality whole-body PET/MR imaging systems.[108] Deconvolution, deblurring, or image restoration can also be applied to improve the image resolution and reduce PVE.[109] The computation load of these approaches tends to be large and may hinder their application in a clinical setting.

Because PET/CT for RT is typically involved with lung cancer and esophageal cancer, tumor motion is another component complicating the correction of PVE. It is difficult if not impossible to separate tumor motion from PVE as far as quantification of the PET data is concerned. **Fig. 9** shows an

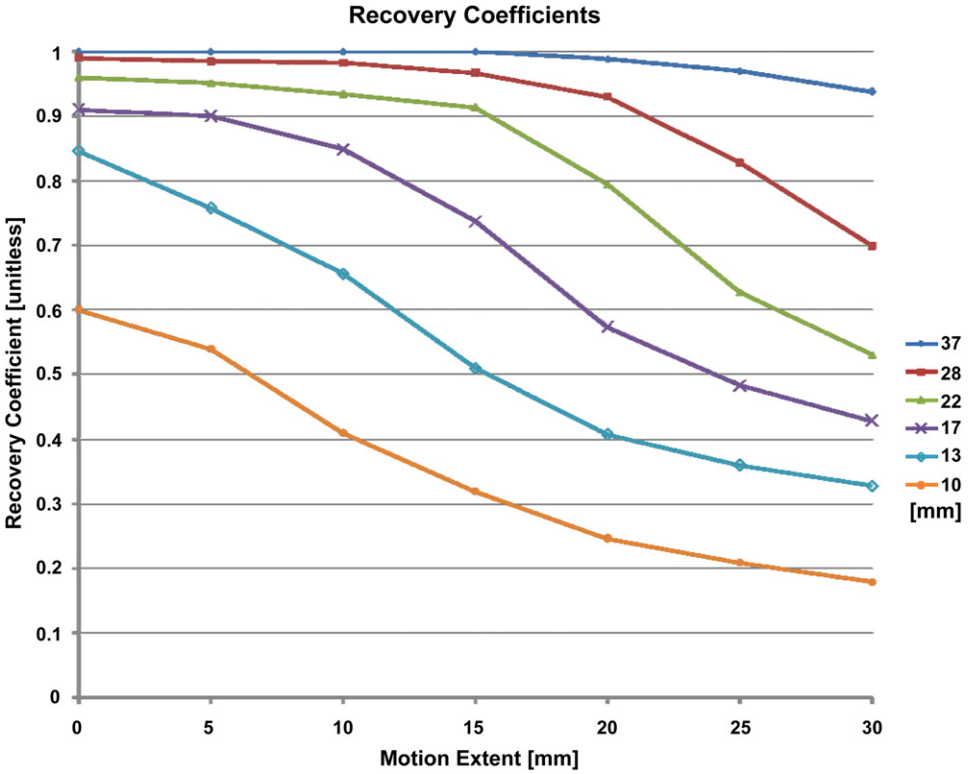

Fig. 9. The recovery coefficients of a PET/CT system measured from a NEMA IEC phantom on a motion platform. There were 6 spheres of size, 10, 13, 17, 22, 28, and 37 mm, and 7 motion amplitudes of 0 to 30 mm in increments of 5 mm. The SBR was 50:1. Each data point was averaged from 3 measurements.

example of RC as a function of different sphere sizes (10, 13, 17, 22, 28, and 37 mm) and various degrees of motion (no motion to 30 mm) by measuring the degradation of a known activity with the image quality phantom IEC phantom at the SBR of 50:1. Tumor motion adds another dimension of degradation on top of the PVE. Incorporation of 4-D CT to help assess the magnitude of tumor motion and the size and shape of the tumor from CT can be helpful in modeling both the tumor motion and system resolution in image reconstruction[110] or image deconvolution[88,111] to simultaneously compensate for both motion and PVE. One such approach applied successfully in the context of oncologic PET imaging uses an iterative 3-D deconvolution algorithm and a local model of the PET scanner's point spread function followed by application of a PVE correction to the mean voxel value within a VOI.[109] The authors report more accurate quantitative assessments of uptake in lesions greater than 1.5 times the PET imaging spatial resolution.

A different, novel type of approach to this problem has been to directly quantify ROIs from projection data, taking the effect of PVE (among others factors such as scatter) into account. Derived from the early work of Huesman,[103] this approach has been developed and investigated in the context of oncologic imaging.[91,112] This method has the particular advantage of being able to estimate region variance for subsequent use in model analysis to obtain parameter estimates; however, this method remains to be extended to 3-D.

PET Image Segmentation

Over the past few years, several methods have been proposed for target volume definition in RTP based on incorporating PET physiologic information. In particular, ^{18}F-FDG-PET is currently used in many cancer centers around the world to improve biologic target volume definition, which is traditionally identified on CT simulation images in RT clinical routine.[113] Accurate volume definition is particularly important in RT because it constitutes the target of the radiation beam; underdosing of tumor may lead to recurrence whereas overdosing of surrounding normal tissues might lead to severe and possibly lethal side effects to patients, such as brain or lung injury.[114] Different approaches can be followed to categorize PET segmentation approaches, including the cancer site, the injected radiotracer, or the image processing technique. There could be differences and overlaps between sites, tracers, or techniques. For many reasons, the authors have opted to categorize PET segmentation based on the techniques used and refer to differences in sites or tracer specific variations as appropriate.[115] There is a plethora of segmentation methods that could be applied to nuclear medicine imaging, particularly in cardiovascular imaging; readers are referred to articles by Boudrass and colleageus.[116,117] According to a literature survey of existing methods, the authors identified 4 broad categories of PET segmentation methodologies: (1) image thresholding methods, (2) variational approaches, (3) learning methods, and (4) stochastic modeling-based techniques.[46] A detailed description of these algorithms is beyond the scope of this review and can be found in that survey.

Thresholding is the most widely used PET segmentation approach in clinical practice for biologic target volume delineation for RTP. The only competing approach with thresholding is possibly visual interpretation of PET scans and identification of lesion boundary by consensus reading of an experienced nuclear medicine physician and radiation oncologist.[118,119] Visual inspection is susceptible to the window-level settings, however, and suffers from interobserver variability. Therefore, several segmentation methods based on thresholding have emerged to reduce this subjectivity. There is a large variability in terms of computational complexity and amount of user interaction required by the various image segmentation techniques. Despite their limitations, visual delineation performed by experts is still the most widely used technique.[8] Manual techniques, however, are labor intensive and suffer from intraobserver variability whereas thresholding techniques are simple to put into practice, although scanner-specific calibration might be required for implementation of the adaptive thresholding method. The high computational burden associated with supervised methods that require time-consuming training is also worth emphasizing. In a clinical setting, the balance between algorithmic complexity and the validity of results obtained is an important criterion when selecting a PET image segmentation technique.

A challenging, even problematic, issue for validation of PET segmentation algorithms, is the identification of a gold standard (ie, benchmark).[120,121] Segmentation methods yield binary classification results (a voxel belongs to the object or does not). There are basically 4 different strategies allowing the assessment of the accuracy of PET image segmentation techniques. The review by Zaidi and El Naqa[46] summarizes these strategies and provides a concise summary of their advantages, drawbacks and limitations. These

include manual segmentation by experts in the field, the use of simulated or experimental phantom studies where the ground truth (tumor volume) is known a priori, the comparison with correlated anatomic GTVs defined on CT or MR imaging, and the comparison of tumor volumes delineated on clinical PET data with actual tumor volumes measured on the macroscopic specimen derived from histology, in case a PET scan was undertaken before surgery. It should be emphasized that such correlative analysis relies on a high degree of registration accuracy between multimodality images, which is still challenging to perform in a clinical setting.[122]

Many studies compared various PET image segmentation techniques using phantom and clinical studies. For example, Vees and colleagues[11] compared various image segmentation techniques in the delineation of GTV in patients with cerebral glioma (**Fig. 10**). The study results highlighted the limitations associated with some of the segmentation algorithms (eg, SUV = 2.5 cutoff and the gradient finding GTV approaches) compared with the SBR-based adaptive thresholding technique and its impact on RT planning in patients of cerebral glioma. The investigators concluded the selection of the most appropriate ^{18}F-FET-PET–based segmentation algorithm is crucial for correct delineation of resulting GTV.[11]

A recent study compared 9 PET image segmentation techniques.[123] These include manual delineation performed by an experienced radiation oncologist on both the CT and PET images, 4 semiautomated methods comprising the SBR-based adaptive thresholding technique,[124] region growing,[125] Black and colleagues' technique,[126] Nestle and colleagues' technique,[127] and 3 fully automated methods: standard fuzzy C-means[128]; spatial FCM, which incorporates nonlinear anisotropic diffusion filtering, thus allowing the integration of spatial contextual information; and the wavelet-based FCM-S algorithm, which also

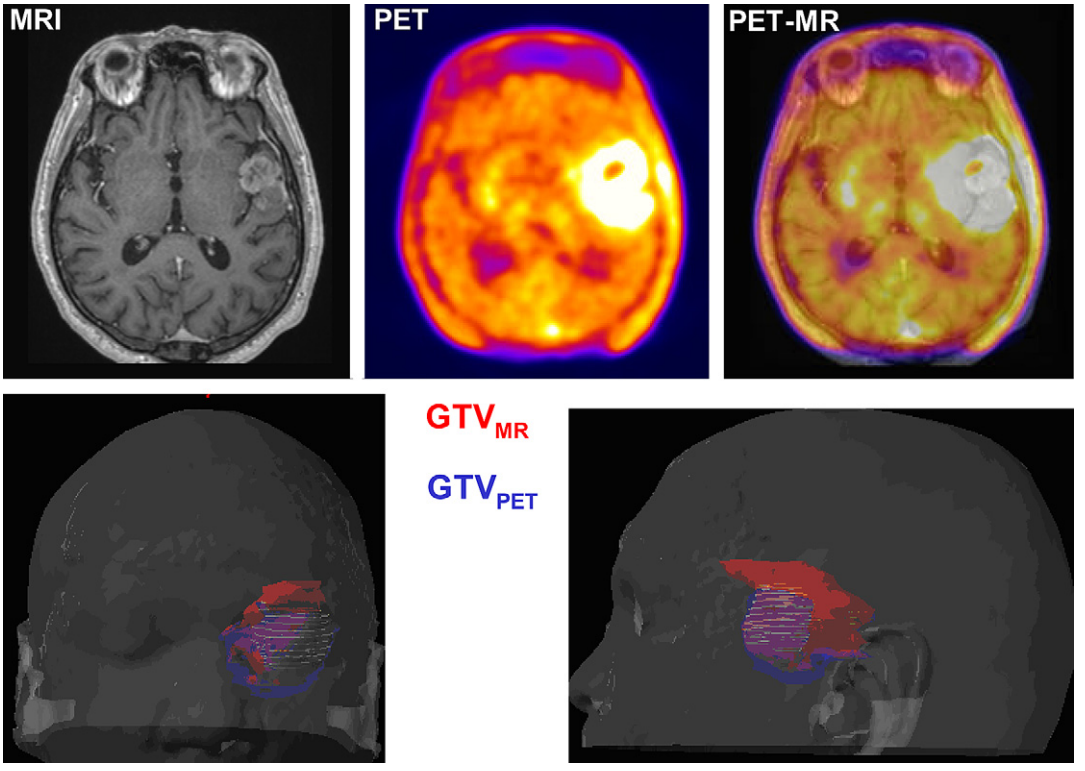

Fig. 10. Typical example of geographic mismatch between GTVs defined on MR imaging and PET for a clinical study with a glioblastoma. (*Top*) From left to right, gadolinium-enhanced T1-weighted MR imaging, corresponding ^{18}F-FET–PET study, and fused PET/MR imaging. (*Bottom*) 3-D rendering illustrating the substantial mismatch. Note that the GTV defined on MR imaging overestimates the tumor extension relative to GTV defined on PET images. (*Adapted from* Weber DC, Zilli T, Buchegger F, et al. [(18)F]fluoroethyltyrosine-positron emission tomography-guided radiotherapy for high-grade glioma. Radiat Oncol 2008;3:44; with permission; and Vees H, Senthamizhchelvan S, Miralbell R, et al. Assessment of various strategies for 18F-FET PET-guided delineation of target volumes in high-grade glioma patients. Eur J Nucl Med Mol Imaging 2009;36:182–93; with permission.)

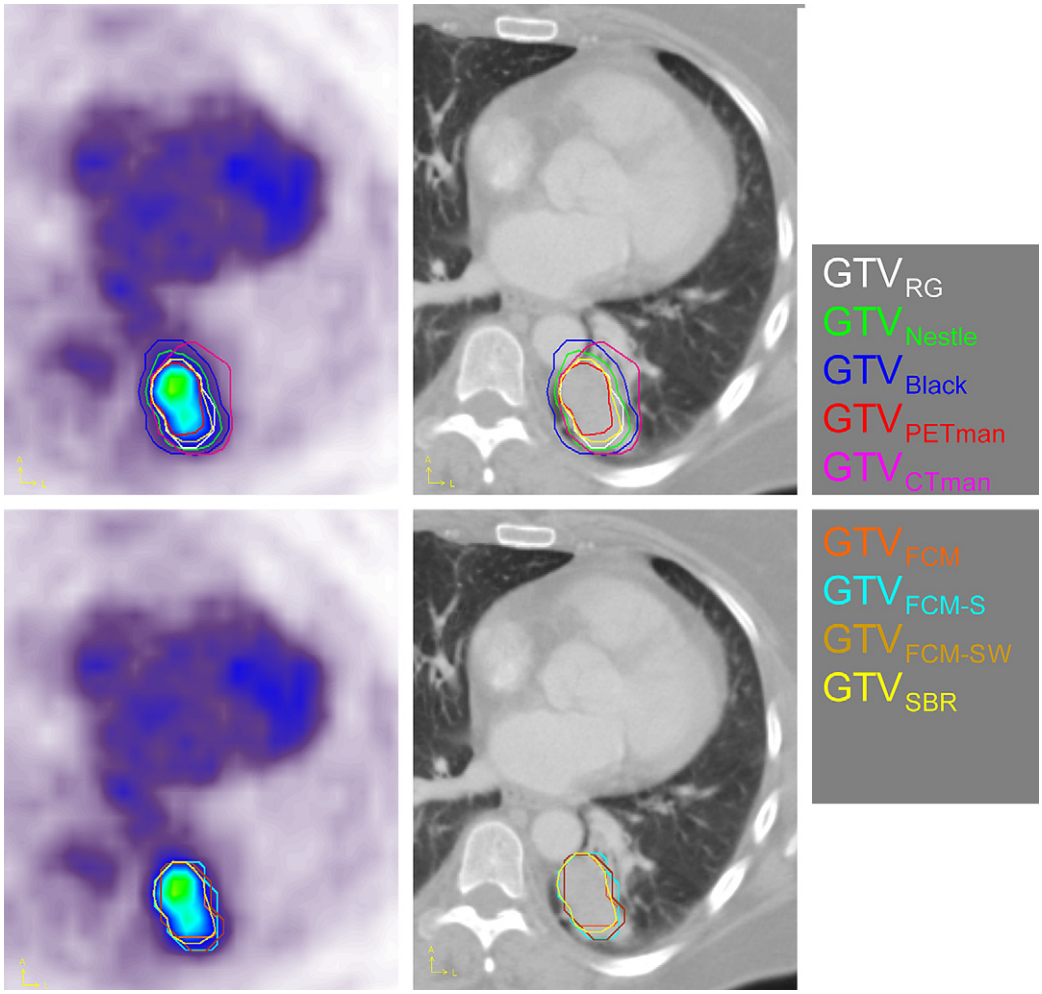

Fig. 11. Representative segmentation results of ^{18}F-FDG-PET/CT image of a patient presenting with histologically proved NSCLC. The gross tumor volumes defined on the ellipsoidal homogeneous lesion using 9 segmentation techniques are depicted on both the CT (*left*) and ^{18}F-FDG-PET (*right*) transaxial slices.

considers inhomogeneity of tracer uptake through the use of the à trou wavelet transform.[129] Representative segmentation results of ^{18}F-FDG-PET/CT image of a patient presenting with histologically proved NSCLC are shown in **Fig. 11**. The GTVs defined on the nonhomogeneous lesion using 9 segmentation techniques are depicted on both the CT (left) and ^{18}F-FDG-PET (right) transaxial slices.

SUMMARY AND FUTURE PERSPECTIVES

There have been many contributions demonstrating the advantages of combining morphologic and molecular imaging in the process of RTP thanks to the widespread acceptance of combined PET/CT scanners. The emergence of novel technologies, including PET/MR imaging, will likely boost further the application of multimodality imaging in RT for various indications. Molecular imaging-guided RT holds the promise of improved delineation of tumor target volumes. Yet, despite considerable progress to date, challenges remain if the potential of PET/CT-guided RTP is to be fully exploited in clinical routine.

PET/CT has been mainly used for whole-body oncologic studies, an application embracing the mainstream of reimbursable indications for PET/CT in the United States and many other countries. Reimbursement issues are mainly driven by prospective multicenter clinical trials that reveal enhancements in health outcomes conveyed by PET/CT as an imaging modality for a given indication. It is expected that ongoing collaborative efforts will allow expanding coverage for PET/CT scans by following the same trend adopted for

other indications, including RTP. The continuing decline of reimbursement coupled with the drop in price of PET/CT scanners are likely to help the application of PET/CT for RT. After all, if the benefit can be demonstrated and if the cost of scans are dropping, the future of PET/CT for RT can only be brighter than it is today.

REFERENCES

1. Bradley J, Thorstad WL, Mutic S, et al. Impact of FDG-PET on radiation therapy volume delineation in non-small-cell lung cancer. Int J Radiat Oncol Biol Phys 2004;59:78–86.
2. Ciernik IF, Dizendorf E, Baumert BG, et al. Radiation treatment planning with an integrated positron emission and computer tomography (PET/CT): a feasibility study. Int J Radiat Oncol Biol Phys 2003;57:853–63.
3. Mah K, Caldwell CB, Ung YC, et al. The impact of (18)FDG-PET on target and critical organs in CT-based treatment planning of patients with poorly defined non-small-cell lung carcinoma: a prospective study. Int J Radiat Oncol Biol Phys 2002;52: 339–50.
4. van Baardwijk A, Baumert BG, Bosmans G, et al. The current status of FDG-PET in tumor volume definition in radiotherapy treatment planning. Cancer Treat Rev 2006;32:245–60.
5. Messa C, Di Muzio N, Picchio M, et al. PET/CT and radiotherapy. Q J Nucl Med Mol Imaging 2006;50: 4–14.
6. Stewart RD, Li XA. BGRT: biologically guided radiation therapy—the future is fast approaching. Med Phys 2007;34:3739–51.
7. Zaidi H, Vees H, Wissmeyer M. Molecular PET/CT imaging-guided radiation therapy treatment planning. Acad Radiol 2009;16:1108–33.
8. Steenbakkers RJ, Duppen JC, Fitton I, et al. Reduction of observer variation using matched CT-PET for lung cancer delineation: a three-dimensional analysis. Int J Radiat Oncol Biol Phys 2006;64:435–48.
9. Ashamalla H, Rafla S, Parikh K, et al. The contribution of integrated PET/CT to the evolving definition of treatment volumes in radiation treatment planning in lung cancer. Int J Radiat Oncol Biol Phys 2005;63:1016–23.
10. Weber DC, Zilli T, Buchegger F, et al. [(18)F]Fluoroethyltyrosine-positron emission tomography-guided radiotherapy for high-grade glioma. Radiat Oncol 2008;3:44.
11. Vees H, Senthamizhchelvan S, Miralbell R, et al. Assessment of various strategies for 18F-FET PET-guided delineation of target volumes in high-grade glioma patients. Eur J Nucl Med Mol Imaging 2009;36:182–93.
12. Erdi YE, Rosenzweig K, Erdi AK, et al. Radiotherapy treatment planning for patients with non-small cell lung cancer using positron emission tomography (PET). Radiother Oncol 2002;62:51–60.
13. Schwartz DL, Ford EC, Rajendran J, et al. FDG-PET/CT-guided intensity modulated head and neck radiotherapy: a pilot investigation. Head Neck 2005;27:478–87.
14. Zaidi H. Quantitative analysis in nuclear medicine imaging. In: Zaidi H, editor. New York: Springer; 2006. p. 564.
15. Zaidi H, Alavi A. Preface. PET Clin 2007;2:xi–xiv.
16. Mankoff D, Shields A, Krohn K. PET imaging of cellular proliferation. Radiol Clin North Am 2005; 43:153–67.
17. Jager PL, Chirakal R, Marriott CJ, et al. 6-L-18F-Fluorodihydroxyphenylalanine PET in neuroendocrine tumors: basic aspects and emerging clinical applications. J Nucl Med 2008;49:573–86.
18. Milker-Zabel S, Zabel-du Bois A, Henze M, et al. Improved target volume definition for fractionated stereotactic radiotherapy in patients with intracranial meningiomas by correlation of CT, MRI, and [68Ga]-DOTATOC-PET. Int J Radiat Oncol Biol Phys 2006;65:222–7.
19. Shapiro B. Ten years of experience with MIBG applications and the potential of new radiolabeled peptides: a personal overview and concluding remarks. Q J Nucl Med 1995;39:150–5.
20. Belvisi L, Bernardi A, Colombo M, et al. Targeting integrins: insights into structure and activity of cyclic RGD pentapeptide mimics containing azabicycloalkane amino acids. Bioorg Med Chem 2006; 14:169–80.
21. Beer AJ, Grosu AL, Carlsen J, et al. [18F]Galacto-RGD positron emission tomography for imaging of {alpha}v{beta}3 expression on the neovasculature in patients with squamous cell carcinoma of the head and neck. Clin Cancer Res 2007;13:6610–6.
22. Couturier O, Luxen A, Chatal JF, et al. Fluorinated tracers for imaging cancer with positron emission tomography. Eur J Nucl Med Mol Imaging 2004; 31:1182–206.
23. Blankenberg F, Katsikis P, Tait J, et al. In vivo detection and imaging of phosphatidylserine expression during programmed cell death. Proc Natl Acad Sci U S A 1998;95:6349–54.
24. Rajendran J, Krohn K. Imaging hypoxia and angiogenesis in tumors. Radiol Clin North Am 2005;43: 169–87.
25. Thorwarth D, Alber M. Implementation of hypoxia imaging into treatment planning and delivery. Radiother Oncol 2010;97:172–5.
26. Weinmann M, Welz S, Bamberg M. Hypoxic radiosensitizers and hypoxic cytotoxins in radiation oncology. Curr Med Chem Anticancer Agents 2003;3:364–74.

27. Vaupel P, Harrison L. Tumor hypoxia: causative factors, compensatory mechanisms, and cellular response. Oncologist 2004;9(Suppl 5):4–9.
28. Padhani A. PET imaging of tumor hypoxia. Cancer Imaging 2006;6:S117–21.
29. Nunn A, Linder K, Strauss HW. Nitroimidazoles and imaging hypoxia. Eur J Nucl Med 1995;22:265–80.
30. Koh WJ, Bergman KS, Rasey JS, et al. Evaluation of oxygenation status during fractionated radiotherapy in human nonsmall cell lung cancers using [F-18]fluoromisonidazole positron emission tomography. Int J Radiat Oncol Biol Phys 1995;33:391–8.
31. Rajendran JG, Wilson DC, Conrad EU, et al. [(18)F] FMISO and [(18)F]FDG PET imaging in soft tissue sarcomas: correlation of hypoxia, metabolism and VEGF expression. Eur J Nucl Med Mol Imaging 2003;30:695–704.
32. Hicks RJ, Rischin D, Fisher R, et al. Utility of FMISO PET in advanced head and neck cancer treated with chemoradiation incorporating a hypoxia-targeting chemotherapy agent. Eur J Nucl Med Mol Imaging 2005;32:1384–91.
33. Dence CS, Ponde DE, Welch MJ, et al. Autoradiographic and small-animal PET comparisons between (18)F-FMISO, (18)F-FDG, (18)F-FLT and the hypoxic selective (64)Cu-ATSM in a rodent model of cancer. Nucl Med Biol 2008;35:713–20.
34. Dehdashti F, Mintun MA, Lewis JS, et al. In vivo assessment of tumor hypoxia in lung cancer with 60Cu-ATSM. Eur J Nucl Med Mol Imaging 2003; 30:844–50.
35. Grigsby PW, Malyapa RS, Higashikubo R, et al. Comparison of molecular markers of hypoxia and imaging with (60)Cu-ATSM in cancer of the uterine cervix. Mol Imaging Biol 2007;9:278–83.
36. Dehdashti F, Grigsby PW, Lewis JS, et al. Assessing tumor hypoxia in cervical cancer by PET with 60Cu-labeled diacetyl-bis(N4-methylthiosemicarbazone). J Nucl Med 2008;49:201–5.
37. Dehdashti F, Grigsby PW, Mintun MA, et al. Assessing tumor hypoxia in cervical cancer by positron emission tomography with 60Cu-ATSM: relationship to therapeutic response-a preliminary report. Int J Radiat Oncol Biol Phys 2003;55:1233–8.
38. Dolbier WR Jr, Li AR, Koch CJ, et al. [18F]-EF5, a marker for PET detection of hypoxia: synthesis of precursor and a new fluorination procedure. Appl Radiat Isot 2001;54:73–80.
39. Komar G, Seppanen M, Eskola O, et al. 18F-EF5: a new PET tracer for imaging hypoxia in head and neck cancer. J Nucl Med 2008;49:1944–51.
40. Evans S, Hahn S, Judy K, et al. 18F EF5 PET imaging with imunohistochemical validation in patients with brain lesions [abstract]. Int J Radiat Oncol Biol Phys 2006;66:S248.
41. Yap JT, Carney JP, Hall NC, et al. Image-guided cancer therapy using PET/CT. Cancer J 2004;10:221–33.
42. Bradley JD, Perez CA, Dehdashti F, et al. Implementing biologic target volumes in radiation treatment planning for non-small cell lung cancer. J Nucl Med 2004;45(Suppl 1):96S–101S.
43. Brunetti J, Caggiano A, Rosenbluth B, et al. Technical aspects of positron emission tomography/computed tomography fusion planning. Semin Nucl Med 2008;38:129–36.
44. Pan T, Mawlawi O. PET/CT in radiation oncology. Med Phys 2008;35:4955–66.
45. Nestle U, Weber W, Hentschel M, et al. Biological imaging in radiation therapy: role of positron emission tomography. Phys Med Biol 2009;54:R1–25.
46. Zaidi H, El Naqa I. PET-guided delineation of radiation therapy treatment volumes: a survey of image segmentation techniques. Eur J Nucl Med Mol Imaging 2010;37:2165–87.
47. Macapinlac HA. Clinical applications of positron emission tomography/computed tomography treatment planning. Semin Nucl Med 2008;38:137–40.
48. Czernin J, Allen-Auerbach M, Schelbert HR. Improvements in cancer staging with PET/CT: Literature-based evidence as of september 2006. J Nucl Med 2007;48:78S–88S.
49. Ling CC, Humm J, Larson S, et al. Towards multidimensional radiotherapy (MD-CRT): biological imaging and biological conformality. Int J Radiat Oncol Biol Phys 2000;47:551–60.
50. Chapman JD, Bradley JD, Eary JF, et al. Molecular (functional) imaging for radiotherapy applications: an RTOG symposium. Int J Radiat Oncol Biol Phys 2003;55:294–301.
51. Paulino AC, Thorstad WL, Fox T. Role of fusion in radiotherapy treatment planning. Semin Nucl Med 2003;33:238–43.
52. Scarfone C, Lavely WC, Cmelak AJ, et al. Prospective feasibility trial of radiotherapy target definition for head and neck cancer using 3-dimensional PET and CT imaging. J Nucl Med 2004; 45:543–52.
53. Osman MM, Cohade C, Nakamoto Y, et al. Clinically significant inaccurate localization of lesions with PET/CT: frequency in 300 patients. J Nucl Med 2003;44:240–3.
54. Beyer T, Antoch G, Muller S, et al. Acquisition protocol considerations for combined PET/CT imaging. J Nucl Med 2004;45(Suppl 1):25S–35S.
55. Goerres GW, Burger C, Schwitter MR, et al. PET/CT of the abdomen: optimizing the patient breathing pattern. Eur Radiol 2003;13:734–9.
56. Pan T, Mawlawi O, Luo D, et al. Attenuation correction of PET cardiac data with low-dose average CT in PET/CT. Med Phys 2006;33:3931–8.
57. Keall PJ, Mageras GS, Balter JM, et al. The management of respiratory motion in radiation oncology report of AAPM Task Group 76. Med Phys 2006; 33:3874–900.

58. Riegel AC, Ahmad M, Sun X, et al. Dose calculation with respiration-averaged CT processed from cine CT without a respiratory surrogate. Med Phys 2008; 35:5738–47.
59. Cai J, Read PW, Baisden JM, et al. Estimation of error in maximal intensity projection-based internal target volume of lung tumors: a simulation and comparison study using dynamic magnetic resonance imaging. Int J Radiat Oncol Biol Phys 2007;69:895–902.
60. Nehmeh SA, Erdi YE, Meirelles GS, et al. Deep-inspiration breath-hold PET/CT of the thorax. J Nucl Med 2007;48:22–6.
61. Nagamachi S, Wakamatsu H, Kiyohara S, et al. The reproducibility of deep-inspiration breath-hold (18) F-FDG PET/CT technique in diagnosing various cancers affected by respiratory motion. Ann Nucl Med 2010;24:171–8.
62. Daisaki H, Shinohara H, Terauchi T, et al. Multi-bed-position acquisition technique for deep inspiration breath-hold PET/CT: a preliminary result for pulmonary lesions. Ann Nucl Med 2010;24:179–88.
63. Torizuka T, Tanizaki Y, Kanno T, et al. Single 20-second acquisition of deep-inspiration breath-hold PET/CT: clinical feasibility for lung cancer. J Nucl Med 2009;50:1579–84.
64. Nagamachi S, Wakamatsu H, Kiyohara S, et al. Usefulness of a deep-inspiration breath-hold 18F-FDG PET/CT technique in diagnosing liver, bile duct, and pancreas tumors. Nucl Med Commun 2009;30:326–32.
65. Kawano T, Ohtake E, Inoue T. Deep-inspiration breath-hold PET/CT of lung cancer: maximum standardized uptake value analysis of 108 patients. J Nucl Med 2008;49:1223–31.
66. Pan T, Mawlawi O, Nehmeh SA, et al. Attenuation correction of PET images with respiration-averaged CT images in PET/CT. J Nucl Med 2005;46:1481–7.
67. Chi PC, Mawlawi O, Luo D, et al. Effects of respiration-averaged computed tomography on positron emission tomography/computed tomography quantification and its potential impact on gross tumor volume delineation. Int J Radiat Oncol Biol Phys 2008;71:890–9.
68. Meirelles GS, Erdi YE, Nehmeh SA, et al. Deep-inspiration breath-hold PET/CT: clinical findings with a new technique for detection and characterization of thoracic lesions. J Nucl Med 2007;48: 712–9.
69. Vogel WV, van Dalen JA, Wiering B, et al. Evaluation of image registration in PET/CT of the liver and recommendations for optimized imaging. J Nucl Med 2007;48:910–9.
70. Osman MM, Cohade C, Nakamoto Y, et al. Respiratory motion artifacts on PET emission images obtained using CT attenuation correction on PET-CT. Eur J Nucl Med Mol Imaging 2003;30:603–6.
71. Goerres GW, Kamel E, Seifert B, et al. Accuracy of image coregistration of pulmonary lesions in patients with non-small cell lung cancer using an integrated PET/CT system. J Nucl Med 2002;43: 1469–75.
72. Goerres GW, Kamel E, Heidelberg TN, et al. PET-CT image co-registration in the thorax: influence of respiration. Eur J Nucl Med Mol Imaging 2002; 29:351–60.
73. Beyer T, Rosenbaum S, Veit P, et al. Respiration artifacts in whole-body (18)F-FDG PET/CT studies with combined PET/CT tomographs employing spiral CT technology with 1 to 16 detector rows. Eur J Nucl Med Mol Imaging 2005;32: 1429–39.
74. Beddar AS, Briere TM, Balter P, et al. 4D-CT imaging with synchronized intravenous contrast injection to improve delineation of liver tumors for treatment planning. Radiother Oncol 2008;87(3): 445–8.
75. Gould KL, Pan T, Loghin C, et al. Frequent diagnostic errors in cardiac PET/CT due to misregistration of CT attenuation and emission PET images: a definitive analysis of causes, consequences, and corrections. J Nucl Med 2007;48:1112–21.
76. Young H, Baum R, Cremerius U, et al. Measurement of clinical and subclinical tumor response using [18F]-fluorodeoxyglucose and positron emission tomography: review and 1999 EORTC recommendations. European Organization for Research and Treatment of Cancer (EORTC) PET Study Group. Eur J Cancer 1999;35:1773–82.
77. Keall P. 4-Dimensional computed tomography imaging and treatment planning. Semin Radiat Oncol 2004;14:81–90.
78. Wahl LM, Asselin MC, Nahmias C. Regions of interest in the venous sinuses as input functions for quantitative PET. J Nucl Med 1999;40:1666–75.
79. Geworski L, Knoop BO, de Cabrejas ML, et al. Recovery correction for quantitation in emission tomography: a feasibility study. Eur J Nucl Med 2000;27:161–9.
80. Degirmenci B, Wilson D, Laymon CM, et al. Standardized uptake value-based evaluations of solitary pulmonary nodules using F-18 fluorodeoxyglucose-PET/computed tomography. Nucl Med Commun 2008;29:614–22.
81. Alessio AM, Kinahan PE, Lewellen TK. Modeling and incorporation of system response functions in 3-D whole body PET. IEEE Trans Med Imaging 2006;25:828–37.
82. Karp JS, Surti S, Daube-Witherspoon ME, et al. Benefit of time-of-flight in PET: experimental and clinical results. J Nucl Med 2008;49:462–70.
83. Soret M, Bacharach SL, Buvat I. Partial-volume effect in PET tumor imaging. J Nucl Med 2007;48: 932–45.

84. Panin VY, Kehren F, Michel C, et al. Fully 3-D PET reconstruction with system matrix derived from point source measurements. IEEE Trans Med Imaging 2006;25:907–21.
85. Qiao F, Pan T, Clark JW Jr, et al. A motion-incorporated reconstruction method for gated PET studies. Phys Med Biol 2006;51:3769–83.
86. Pan T, Lee TY, Rietzel E, et al. 4D-CT imaging of a volume influenced by respiratory motion on multi-slice CT. Med Phys 2004;31:333–40.
87. Manning K, Tepfer B, Goldklang G, et al. Clinical practice guidelines for the utilization of positron emission tomography/computed tomography imaging in selected oncologic applications: suggestions from a provider group. Mol Imaging Biol 2007;9:324–32 [discussion: 323].
88. El Naqa I, Low DA, Bradley JD, et al. Deblurring of breathing motion artifacts in thoracic PET images by deconvolution methods. Med Phys 2006;33: 3587–600.
89. Werner MK, Parker JA, Kolodny GM, et al. Respiratory gating enhances imaging of pulmonary nodules and measurement of tracer uptake in FDG PET/CT. AJR Am J Roentgenol 2009;193:1640–5.
90. Rahmim A, Tang J, Zaidi H. Four-dimensional (4D) image reconstruction strategies in dynamic PET: beyond conventional independent frame reconstruction. Med Phys 2009;36:3654–70.
91. Schoenahl F, Zaidi H. Towards optimal model-based partial volume effect correction in oncological PET imaging. Proceedings of IEEE Nuclear Science Symposium & Medical Imaging Conference. Rome, Italy, October 19–22, 2004. p. 3177–81.
92. Suckling J, Ott RJ, Deehan BJ. Quantitative analysis of a reconstruction method for fully three-dimensional PET. Phys Med Biol 1992;37:751–66.
93. Townsend DW. Positron emission tomography/computed tomography. Semin Nucl Med 2008;38: 152–66.
94. Rousset O, Rahmim A, Alavi A, et al. Partial volume correction strategies in PET. PET Clin 2007;2: 235–49.
95. Hoffman EJ, Huang SC, Phelps ME. Quantitation in positron emission computed tomography: 1. Effect of object size. J Comput Assist Tomogr 1979;3: 299–308.
96. Kessler RM, Ellis JR Jr, Eden M. Analysis of emission tomographic scan data: limitations imposed by resolution and background. J Comput Assist Tomogr 1984;8:514–22.
97. Avril N, Bense S, Ziegler SI, et al. Breast imaging with fluorine-18-FDG PET: quantitative image analysis. J Nucl Med 1997;38:1186–91.
98. Menda Y, Bushnell DL, Madsen MT, et al. Evaluation of various corrections to the standardized uptake value for diagnosis of pulmonary malignancy. Nucl Med Commun 2001;22:1077–81.
99. Hickeson M, Yun M, Matthies A, et al. Use of a corrected standardized uptake value based on the lesion size on CT permits accurate characterization of lung nodules on FDG-PET. Eur J Nucl Med Mol Imaging 2002;29:1639–47.
100. Reader AJ, Zaidi H. Advances in PET image reconstruction. PET Clinics 2007;2:173–90.
101. Da Silva AJ, Tang HR, Wong KH, et al. Absolute quantification of regional myocardial uptake of 99mTc-sestamibi with SPECT: experimental validation in a porcine model. J Nucl Med 2001;42:772–9.
102. Baete K, Nuyts J, Van Paesschen W, et al. Anatomical-based FDG-PET reconstruction for the detection of hypo-metabolic regions in epilepsy. IEEE Trans Med Imaging 2004;23:510–9.
103. Huesman RH. A new fast algorithm for the evaluation of regions of interest and statistical uncertainty in computed tomography. Phys Med Biol 1984;29:543–52.
104. Carson RE. A maximum likelihood method for region-of-interest evaluation in emission tomography. J Comput Assist Tomogr 1986;10:654–63.
105. Formiconi AR. Least squares algorithm for region of interest evaluation in emission tomography. IEEE Trans Med Imaging 1993;12:90–100.
106. Vanzi E, De Cristofaro M, Ramat S, et al. A direct ROI quantification method for inherent PVE correction: accuracy assessment in striatal SPECT measurements. Eur J Nucl Med Mol Imaging 2007;34:1480–9.
107. Baete K, Nuyts J, Van Laere K, et al. Evaluation of anatomy based reconstruction for partial volume correction in brain FDG-PET. Neuroimage 2004; 23:305–17.
108. Zaidi H, Ojha N, Morich M, et al. PET performance of the Ingenuity TF PET-MR: a whole body PET-MRI system. Phys Med Biol 2011;56:3091–106.
109. Teo BK, Seo Y, Bacharach SL, et al. Partial-volume correction in PET: validation of an iterative postreconstruction method with phantom and patient data. J Nucl Med 2007;48:802–10.
110. Qiao F, Pan T, Clark JW Jr, et al. Joint model of motion and anatomy for PET image reconstruction. Med Phys 2007;34:4626–39.
111. Boussion N, Cheze Le Rest C, Hatt M, et al. Incorporation of wavelet-based denoising in iterative deconvolution for partial volume correction in whole-body PET imaging. Eur J Nucl Med Mol Imaging 2009;36:1064–75.
112. Chen CH, Muzic RF Jr, Nelson AD, et al. Simultaneous recovery of size and radioactivity concentration of small spheroids with PET data. J Nucl Med 1999;40:118–30.
113. Evans PM. Anatomical imaging for radiotherapy. Phys Med Biol 2008;53:R151–91.
114. Perez CA. Principles and practice of radiation oncology. 4th edition. Lippincott Williams & Wilkins, Philadelphia; 2004.

115. Basu S. Selecting the optimal image segmentation strategy in the era of multitracer multimodality imaging: a critical step for image-guided radiation therapy. Eur J Nucl Med Mol Imaging 2009;36: 180–1.
116. Boudraa A, Zaidi H. Image segmentation techniques in nuclear medicine imaging. In: Zaidi H, editor. Quantitative analysis of nuclear medicine images. New York: Springer; 2006. p. 308–57.
117. Boudraa A, Cexus JC, Zaidi H. Functional segmentation of dynamic nuclear medicine images by cross-PsiB energy operator. Comput Meth Prog Biomed 2006;84:148–54.
118. Kiffer JD, Berlangieri SU, Scott AM, et al. The contribution of 18F-fluoro-2-deoxy-glucose positron emission tomographic imaging to radiotherapy planning in lung cancer. Lung Cancer 1998;19:167–77.
119. Wang H, Vees H, Miralbell R, et al. 18F-choline PET-based target volume delineation techniques for partial prostate reirradiation in local recurrent prostate cancer. Radiother Oncol 2009;93:220–5.
120. Zaidi H. Medical image segmentation: Quo Vadis. Comput Meth Prog Biomed 2006;84:63–7.
121. Jannin P, Krupinski E, Warfield S. Guest editorial validation in medical image processing. IEEE Trans Med Imaging 2006;25:1405–9.
122. Slomka P, Baum R. Multimodality image registration with software: state-of-the-art. Eur J Nucl Med Mol Imaging 2009;36:44–55.
123. Belhassen S, Llina Fuentes CS, Dekker A, et al. Comparative methods for 18F-FDG PET-based delineation of target volumes in non-small-cell lung cancer [abstract]. J Nucl Med 2009;50:27P.
124. Daisne JF, Sibomana M, Bol A, et al. Tri-dimensional automatic segmentation of PET volumes based on measured source-to-background ratios: influence of reconstruction algorithms. Radiother Oncol 2003;69:247–50.
125. Graves EE, Quon A, Loo BW Jr. RT_Image: an open-source tool for investigating PET in radiation oncology. Technol Cancer Res Treat 2007;6:111–21.
126. Black QC, Grills IS, Kestin LL, et al. Defining a radiotherapy target with positron emission tomography. Int J Radiat Oncol Biol Phys 2004; 60:1272–82.
127. Nestle U, Kremp S, Schaefer-Schuler A, et al. Comparison of different methods for delineation of 18F-FDG PET-positive tissue for target volume definition in radiotherapy of patients with non-Small cell lung cancer. J Nucl Med 2005;46: 1342–8.
128. Boudraa AE, Champier J, Cinotti L, et al. Delineation and quantitation of brain lesions by fuzzy clustering in positron emission tomography. Comput Med Imaging Graph 1996;20:31–41.
129. Belhassen S, Zaidi H. A novel fuzzy C-means algorithm for unsupervised heterogeneous tumor quantification in PET. Med Phys 2010;37:1309–24.